Resonant Topographic Response of Nearshore Currents to Wind Forcing

T. J. SIMONS

National Water Research Institute, Canada Centre for Inland Waters, Burlington, Ontario, Canada L7R 4A6

(Manuscript received 3 August 1982, in final form 3 November 1982)

ABSTRACT

Model calculations and current meter observations are analyzed in the spectral domain and in the time domain to investigate effects of topographic waves on the response of nearshore currents to wind. The spectral response is computed for a shelf forced by a progressive atmospheric wave, and effects of friction and alongshore depth variations are considered. Comparisons are made with results for standing atmospheric waves and with the response of closed basins forced by winds uniform in space and periodic in time. It is found that coastline curvature is rather unimportant for the scales under consideration, and that the alongshore wind component represents the crucial forcing. Spectral model results are then compared with current meter spectra to show the resonant topographic wave character of the response of currents to wind.

Time series of observed and computed nearshore currents are compared, and the alongshore momentum balances are considered for models with and without topographic wave effect. It is found that simple models may produce results which seem comparable to those obtained from more complete models, but it is concluded that such simple models are basically erroneous in concept.

1. Introduction

Observed current fluctuations in homogeneous coastal waters are often strikingly similar to shore-based wind measurements. This would suggest that the response to wind may, in first approximation, be modeled by a simple momentum balance between alongshore current accelerations, wind stress, bottom friction and, perhaps, a quasi-steady pressure gradient caused by surface set-up. The apparent success of this type of model has led some authors to conclude that observed fluctuations in nearshore currents are essentially consistent with forcing by local wind (Hickey, 1981). Indeed, statistical analysis of time series of individual terms in the alongshore momentum equation confirms that velocity fluctuations as well as pressure gradients are significantly correlated with the local wind stress (Allen and Smith, 1981). On the other hand, analysis of such currents in the frequency domain usually produces energy spectra and coherences consistent with the presence of continental shelf waves recently reviewed by Mysak (1980).

Similar observations and model results for closed basins have been reviewed by Simons (1980). Verification of numerical models of Lake Ontario and the Baltic Sea clearly demonstrate the significant response of nearshore currents to variations in local winds. However, during periods of calm weather, and particularly after a strong wind impulse, the same studies show important effects of topographic modes of oscillation with corresponding reversals of alongshore currents. Again, a spectral analysis of current meter data confirms the prominent contributions from such topographic modes (Saylor *et al.*, 1980).

It follows that observed nearshore current fluctuations cannot be modeled satisfactorily by either a simple momentum balance without wave effects, or a free wave model without wind forcing. Just like the familiar storm surge problem, the response of nearshore currents to wind is a combination of a directly-forced and a free response and hence resonance must occur at forcing frequencies corresponding to any one of the normal modes. This is, of course, clearly demonstrated by a normal mode decomposition of the forced problem as done by Gill and Schumann (1974). Such forced-wave models can explain peaks in current spectra at frequencies different from those in the wind spectra and time lags between response and forcing depending on frequency (see, e.g., Clarke, 1977). It should be noted, however, that differences in the results from forced-wave models and simple momentum-balance models may be much less spectacular in the time domain than in the frequency domain. In fact, it may be possible to adjust the model parameters in a simple momentum balance such that the correlations between observed and computed currents are not significantly lower than those obtained from the forced-wave model, and hence one might obtain the right answer for the wrong reasons.

The present study is an attempt to clarify the various effects entering into the response of barotropic nearshore currents to varying wind stress. The investigation is based on observations in Lake Ontario where the forcing and other environmental conditions may be considered simpler, or in any case, more precisely known, than on the continental shelves. Before proceeding to actual model verification, some idealized model experiments are described to illus-

trate effects of friction and alongshore depth variations on forced topographic waves. Comparisons of model results with observations are made in the spectral domain and in the time domain, and the alongshore momentum balances of models with and without topographic waves are compared.

2. Equations

The governing equations are the linearized, hydrostatic, vertically-integrated equations for homogeneous water without horizontal diffusion and with constant Coriolis parameter f. The scale length L is assumed to be sufficiently smaller than C_0/f, where C_0 is the free surface wave speed, for the rigid-lid approximation to be valid, thus allowing the transport components to be written in terms of a streamfunction. The resulting vorticity equation for the vertically-averaged flow is then

$$\frac{\partial}{\partial t}\nabla\cdot(H^{-1}\nabla\psi) - fJ(H^{-1},\psi) + \nabla\cdot(b\nabla\psi) = \mathrm{curl}(H^{-1}\tau_s\rho^{-1}), \quad (1)$$

where t is time, x and y are the horizontal coordinates with the x-axis directed alongshore and the y-axis offshore, ψ the streamfunction, H the depth, b a depth-dependent bottom friction coefficient, τ_s the wind stress vector, ρ the water density, ∇ the horizontal gradient operator and J the Jacobian.

The vertically-integrated transport components are related to the streamfunction as

$$U = -\frac{\partial\psi}{\partial y}, \quad V = \frac{\partial\psi}{\partial x}. \quad (2)$$

The bottom friction is a slightly simplified version of the familiar Ekman formulation for quasi-steady motion in water of finite depth (see, e.g., Simons, 1980),

$$b = \frac{\alpha f/\Delta}{\alpha^2 + (\delta-\beta)^2}, \quad (3)$$

where Δ is an Ekman depth defined as $\Delta = (\nu/2f)^{1/2}$, where ν is the vertical eddy viscosity, $\delta = H/\Delta$ and

$$\alpha = \frac{\sinh\delta - \sin\delta}{\cosh\delta + \cos\delta}, \quad \beta = \frac{\sinh\delta + \sin\delta}{\cosh\delta + \cos\delta}.$$

For large water depth, this formulation reduces to the well-known deep-ocean value, $b = f\Delta/H^2 = (\nu f/2)^{1/2}H^{-2}$, but for shallow water the coefficient becomes $b = 6f\Delta^2H^{-3} = 3\nu H^{-3}$, thus substantially increasing the drag when the depth becomes of the same order as the Ekman depth.

For the case of a straight shore, the wind is taken to be uniform across the shelf, periodic along the shore and blowing parallel to the shoreline. For the case of a closed basin, the wind is uniform over the whole basin. For the computations in the spectral domain, the wind stress and the streamfunction are written in the form

$$\tau_s = \hat{\tau}_s(x)e^{-i\sigma t}, \quad \psi = \hat{\psi}(x,y)e^{-i\sigma t}, \quad (4)$$

and Eq. (1) becomes

$$\nabla\cdot[(b - i\sigma H^{-1})\nabla\hat{\psi}] - fJ(H^{-1},\hat{\psi}) = \mathrm{curl}(H^{-1}\hat{\tau}_s\rho^{-1}). \quad (5)$$

This equation can be represented by a system of finite-difference equations on a spatial grid and then solved by matrix inversion or relaxation. Once the streamfunction has been determined, the alongshore current follows from (2). The frequency response has an amplitude and a phase. The amplitude is expressed in units of current (m s^{-1}) divided by wind stress (N m^{-2}). The phase is converted to the lag of the current behind the wind in units of the forcing period.

Solutions will be discussed for the following cases. First, effects of bottom friction will be illustrated for an infinitely long, uniform shelf forced by a progressive atmospheric wave. Next, effects of alongshore depth variation are included in this problem, thus requiring a two-dimensional numerical discretization of Eq. (5). Then, the progressive wave forcing in the uniform shelf problem is replaced by a standing atmospheric wave and the results are compared with a circular basin forced by a wind uniform in space and periodic in time. In the final idealized example, the above effects are combined by obtaining two-dimensional numerical solutions for an elongated basin with asymmetric bottom profiles.

The above results are then compared with observations by using a two-dimensional numerical model of Lake Ontario. Comparisons are made in the spectral domain and in the time domain. The alongshore momentum balance is also considered and compared with simpler models.

3. Bottom friction

For an infinitely long uniform shelf and in the absence of wind and bottom friction, the solutions to (5) are the familiar shelf waves propagating in positive x-direction, i.e., with the shore on the right. A periodic wind which is uniform across the shelf and blows alongshore will, in principle, generate all the cross-shore shelf wave modes of the same alongshore wavenumber as the wind. The amplitude equation for each mode may be found by expanding the forcing in terms of these normal modes (Gill and Schumann, 1974). Whenever the forcing frequency becomes equal to one of the normal mode frequencies, resonance occurs and the phase of the response shifts by half a period such that the nearshore current lags behind the wind for higher frequencies and is ahead of the wind for lower frequencies (see also, Allen, 1980).

While the sea-level response is primarily determined by the first few modes (Gill and Schumann, 1974), the same does not hold for the alongshore velocity in the presence of realistic depth profiles near the coast. For example, the solution for a circular basin with parabolic depth (Birchfield and Hickie, 1977) requires a great many radial modes to represent the current in response to wind. However, effects of friction become more important with increasing period and decreasing depth as seen from the first term of (5) where the coefficient b is inversely proportional to the third power of the depth. This is the reason why the higher modes with their longer periods and large nearshore amplitudes contribute less to the overall response than the first cross-shore mode and hence are less likely to show up in the current spectra.

The foregoing may be illustrated by the example of an exponential shelf coupled to a linear depth variation nearshore without discontinuities in depth or slope:

$$\left.\begin{aligned} H/H_0 &= \exp(\alpha y/L), \quad \text{for} \quad 1 > y/L > \alpha^{-1} \\ H/H_0 &= (\alpha y/L)\exp(1), \quad \text{for} \quad y/L < \alpha^{-1} \end{aligned}\right\}, \quad (6)$$

where L is taken to be 100 km, H_0 is set equal to 100 m, and $\alpha = 3$, which approximates the Oregon shelf. The wind stress is taken to have the form of a progressive wave, moving in positive x-direction, with a wavelength of 3000 km which corresponds to atmospheric cyclone scales. The resulting one-dimensional form of Eq. (5) is solved by numerical methods with a gridmesh of 1 km and inversion of the tridiagonal matrix.

Fig. 1 shows the response of the alongshore current as a function of frequency and distance offshore for Ekman depths of 5 m (left) and 10 m (right), respectively. For periods shorter than the first normal mode period (~9 days), offshore currents lag behind nearshore currents and the amplitude response gradually increases with period while the phase lag decreases. The peak of the amplitude response shows a shift from longer to shorter periods when approaching the shore. Beyond the first mode period, the currents are ahead of the forcing and the amplitudes decrease. This corresponds to the phase shift of half a period in the absence of friction. On approaching the second mode period (~33 days), the nearshore current amplitude increases again if the friction is sufficiently weak and its phase tends towards the positive lag of the inviscid solution. In this frequency range, the offshore current is ahead of the nearshore current unlike the solution presented by Brink and Allen (1978). In the present context the important result is that the response which is most likely to be observed is the first mode resonance with a slight phase lag of the alongshore current behind the local wind.

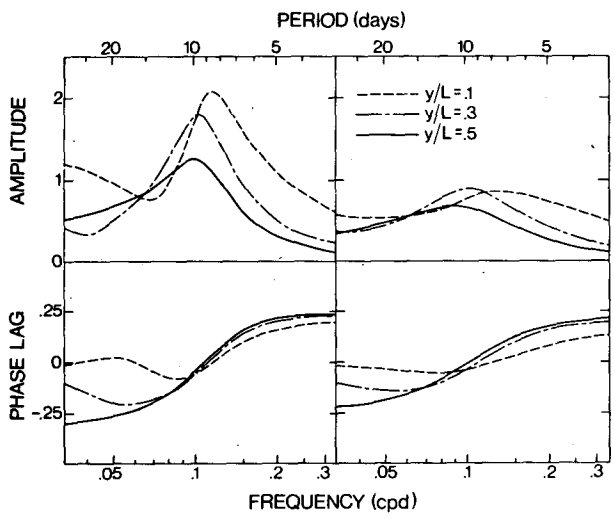

FIG. 1. Response of alongshore current to progressive wind forcing for shelf given by Eq. (6), wavelength 3000 km and Ekman depths of 5 m (left) and 10 m (right).

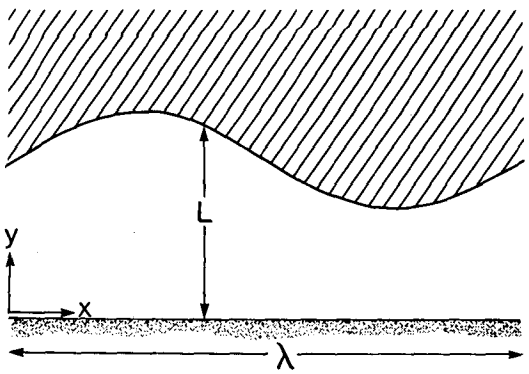

FIG. 2. Idealized shelf with periodic alongshore depth variation in coastal zone of width L and constant depth in shaded area.

4. Alongshore depth variation

When trying to match observed peaks in current spectra to shelf wave dispersion curves, the choice of bottom profile is generally not a simple matter because natural basins or shelves tend to show considerable alongshore depth variations. The effects of such variations on free shelf waves have been discussed by Wang (1980) and others (see, e.g., Mysak, 1980). The corresponding effects on the resonant response to wind forcing will be considered here.

It is assumed that both the forcing and the depth variations are periodic in alongshore direction over the interval λ, thus giving rise to cyclic boundary conditions. In the particular case to be presented here, the wind consists of a progressive wave moving in positive x-direction and having the same wavelength as the alongshore variation of the shelf width L illustrated in Fig. 2. In view of subsequent comparisons with closed basin, the exponential shelf profile of the foregoing example is replaced by a parabolic profile.

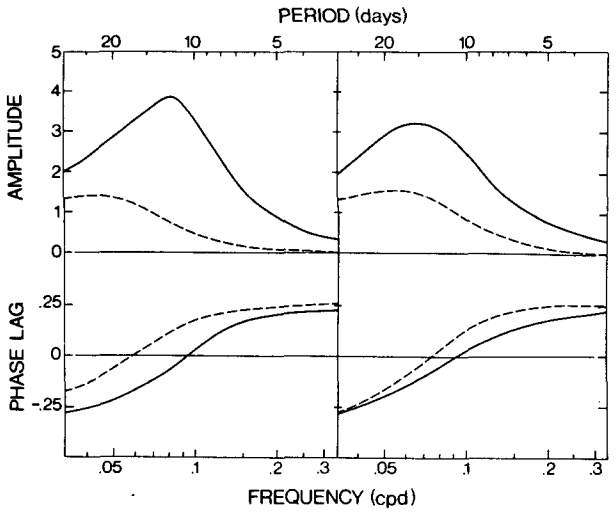

FIG. 3. Response of alongshore current to progressive wind forcing for coastal zone with parabolic depth variation. Left: one-dimensional models with uniform coastal widths of 40 km (solid line) and 20 km (dashed), respectively. Right: results from two-dimensional model of Fig. 2 at location of maximum (solid line) and minimum (dashed) coastal width. Wavelength 400 km, maximum depth 150 m, Ekman depth 1 m, offshore distance 10 km.

$$H/H_0 = 1 - (1 - y/L)^2, \quad \text{for} \quad y/L < 1, \qquad (7)$$

where the width of the shore zone L and the depth of the deep water region H_0, are periodic functions of the alongshore coordinate with wavelength λ. The model parameters are assigned values applicable to the Great Lakes with H_0 = 150 m and L varying between 20 and 40 km. The wavelength applicable to a closed basin is determined by the circumference of the basin rather than the scale of the atmospheric forcing. The value selected here is λ = 400 km. The Ekman depth is taken to be 1 m.

In order to properly evaluate effects of alongshore depth variations it is necessary to first compute response curves for corresponding shelves with uniform profiles. In the present case such computations are done for constant coastal widths L, equal to 40 and 20 km, respectively. The resulting alongshore currents at 10 km offshore are shown on the left of Fig. 3 with the solid curves representing the wide coastal zone and the dashed curves representing the narrow coastal width. The corresponding normal mode periods may be estimated from Ball's (1967) solution for a similar profile which shows that the periods are much longer for the narrow zone than for the wide zone. With regard to the amplitudes it may be noted that streamfunctions for the inviscid case are independent of the scale depth H_0, while the velocities are inversely proportional to depth. Since the same value, H_0 = 150 m, is used in both cases, the velocities at a fixed distance offshore are greater for the wide coastal zone (solid lines). If the scale depth for the narrow shore zone is reduced to H_0 = 90 m so as to produce the same depth at 10 km offshore as the wide zone with H_0 = 150 m, the inviscid current will increase in magnitude but the increase is mostly canceled again by increasing friction in shallow water. In either case, therefore, the amplitude response is smaller for the narrow coastal zone than for the wide one.

The solutions for periodic alongshore depth variation are illustrated on the right of Fig. 3. The solid curves refer to the location where the coastal zone reaches its maximum width, the dashed curves apply to the location of minimum width. As before, the phase lag refers to the local wind. The numerical solutions were obtained on a two-dimensional grid with a mesh size of 4 km. For the one-dimensional case on the left of Fig. 3 such coarse-grid solutions were compared with results from a 1-km mesh and found to be in reasonable agreement.

By comparing the left side of Fig. 3 with the rhs, it is seen that the resonance periods tend to shift toward one another in the presence of alongshore depth variations. This result can, of course, be interpreted in terms of a two-dimensional normal mode for this particular topography. A detailed illustration of the response as a function of alongshore distance is provided by Fig. 4 for three forcing periods near the resonant response, T = 10, 15 and 20 days, respectively. On the basis of these results, one must expect some alongshore variation of resonance frequencies for coastal zones with alongshore depth variations. Also, at a given forcing frequency, it is indicated that the phase lag will vary alongshore and hence the forced shelf wave will appear to propagate with non-uniform speed. However, both variations in resonance periods and in phase lags would be considerably smaller than expected from calculations for a range of shelves with different depth profiles but, in each case, uniform in alongshore direction.

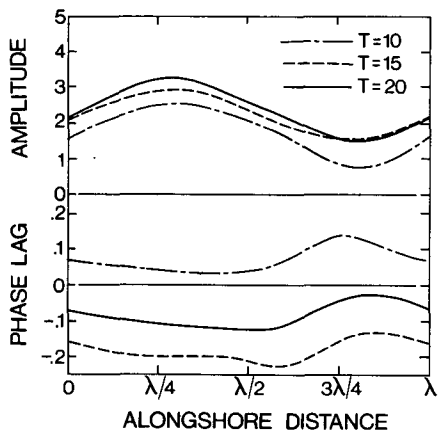

FIG. 4. Alongshore variation of alongshore current for periodic wind forcing with forcing periods T. Model of Fig. 2 with model parameters of Fig. 3.

5. Forcing by standing wave

It is known that meteorological disturbances at middle latitudes tend to progress from west to east rather than from south to north. It is therefore suggested that the response to wind of continental shelves oriented in a north–south direction may be profitably analyzed on the basis of standing rather than progressive atmospheric waves.

A similar situation arises when a lake or inland sea is subjected to meteorological forcing which is generally of such a large scale that it can be treated as uniform over the basin. For the nearshore zone around the perimeter of the basin, the uniform forcing translates into forcing by a standing wave with wavelength equal to the circumference of the basin, i.e., the first azimuthal wavenumber. It is therefore of interest to compare the response to such forcings with the foregoing response to progressive atmospheric waves.

A standing wave may be represented by the sum of two progressive waves with equal amplitudes and moving in opposite directions. Since resonance occurs only for the force moving in the same direction as the shelf wave, the resonant response will be similar to that considered before, but the amplitude will be reduced by one half. The phase lag between the response and the local forcing, however, now depends on the alongshore position even for a uniform shelf profile. It is, in general, similar to the foregoing at the location where the force reaches its maximum and it increases alongshore in the direction of shelf-wave propagation.

To illustrate shelf wave response to standing atmospheric waves while at the same time allowing a direct comparison with the response of closed basins to wind, we consider an infinitely long, uniform channel with parabolic depth variation. The channel is symmetric such that the width of the coastal zone L, defined in (7), is equal to half the width of the channel. The channel width is taken to be 80 km which makes L equal to 40 km, the maximum depth H_0 equals 150 m, the Ekman depth again equals 1 m, and the wavelength of the forcing is 400 km. The response of the alongshore current is presented on the left side of Fig. 5. The alongshore location is the point where the wind reaches its maximum; the offshore locations are at 2, 6, and 10 km from the shore, represented by dashed, dash-dot and solid curves, respectively.

Let us compare this with a circular basin with depth varying with radius only and forced by a wind stress uniform in space and periodic in time. In polar coordinates, the corresponding form of Eq. (1) is quite similar to the equation for a straight shelf forced by a standing atmospheric wave of the form $\tau_{sx} = \tau_0 \sin\sigma t \sin\theta$ where $\theta = 2\pi x\lambda^{-1}$ with x measuring the alongshore distance in counterclockwise direction

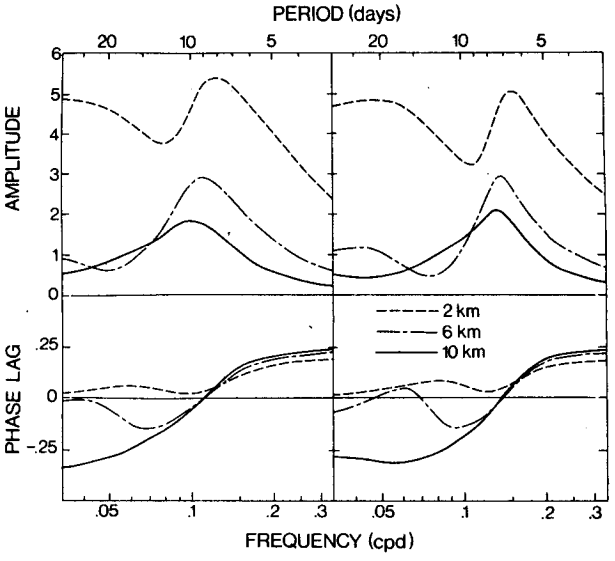

FIG. 5. Alongshore current at location of maximum alongshore component of standing wind forcing. Left: symmetric channel with parabolic depth variation and width of 80 km forced by standing atmospheric wave with wavelength of 400 km. Right: circular basin with radius of 65 km and parabolic depth variation in coastal zone of 40 km, subjected to wind uniform in space and periodic in time. Maximum depth 150 m, Ekman depth 1 m.

from the upwind end of the basin and λ being the circumference of the basin. It follows that the only normal modes which are excited are those corresponding to the first azimuthal wavenumber. For a circular basin with parabolic depth variation for which the rigid lid approximation is valid, these normal modes have periods equal to $2n(n + 2) + 1$ times the inertial period, where n is the radial mode number (see, e.g., Birchfield and Hickie, 1977). Saylor *et al.* (1980) have discussed effects of different depth profiles but their discussion is restricted to the first radial wavenumber.

In the present example, the depth is taken to have the parabolic form (7) in the shore zones and to be constant in the interior. Note that the area of constant depth tends to increase the normal mode periods as compared to the above values for the basin with parabolic depth. The width of the shore zone L is equal to 40 km and the total radius is 65 km, which makes the circumference a little more than 400 km, equivalent to the wavelength in the above example. The maximum depth is $H_0 = 150$ m, the Ekman depth is 1 m, and the numerical solution is obtained on a radial finite-difference grid with a mesh size of 1 km. The response of the alongshore current to a wind uniform in space and periodic in time is shown on the rhs of Fig. 5. The alongshore location is the point where the alongshore component of the wind reaches its maximum, i.e., $\theta = \pi/2$. The offshore locations are the same as those on the lhs of Fig. 5. The response curves on the left and right of Fig. 5 are seen to be

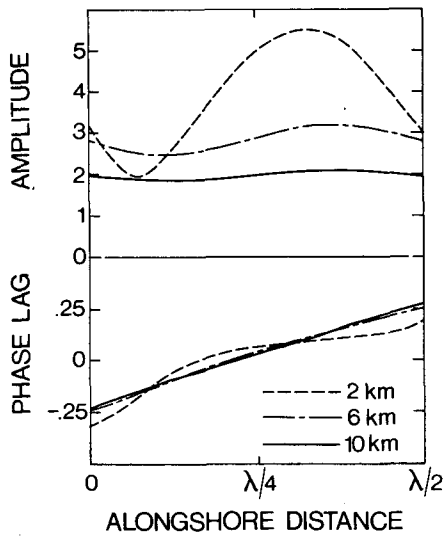

FIG. 6. Alongshore variation of alongshore current in circular basin at forcing period of 7 days. Alongshore distance measured counterclockwise from upwind shore. Model parameters of Fig. 5; λ = circumference.

quite similar, but the resonance period in the circular configuration is somewhat shorter because the effective wavelength is shorter than the circumference of the basin. This shows that coastline curvature is rather unimportant and that the alongshore wind component is the crucial forcing (see also, Clarke, 1977).

To illustrate the alongshore variation of the response, Fig. 6 shows results for the circular basin for a forcing period of 7 days, close to the resonant response, with alongshore distance expressed in terms of the circumference λ. Similar results apply to the case of a straight shore forced by a standing atmospheric wave of wavelength λ. It is apparent that the offshore current is governed by resonant wave propagation with constant amplitude and linear phase change alongshore. On the other hand, the nearshore response appears as a standing wave with a slight counterclockwise shift of the current maxima similar to the steady state solution (Birchfield, 1973). In terms of alongshore phase propagation, the nearshore current exhibits an alongshore variation somewhat similar to the amplitude variation of the forcing with large apparent phase speeds occurring at the location of maximum alongshore wind. Hence, even at resonance, the nearshore phase propagation observed under conditions of standing atmospheric wave forcing, cannot be related to free shelf wave propagation.

It is, perhaps, of interest to note here that the above normal modes for a circular basin differ from typical shelf waves in the sense that the associated currents in deep water are here of the same order of magnitude as in the shore zone. While this point has been emphasized by Saylor *et al.* (1980), it does not affect the discussion of nearshore currents.

6. Elongated asymmetric basin

As a final example, we consider an elongated basin with either latitudinal or longitudinal asymmetry as illustrated by Figs. 7a and b, respectively. The depth variation is again parabolic in the coastal zones and constant in the shaded areas. The wind is directed along the axis of the basin and is uniform in space and periodic in time. The radius of the end circle is equal to 40 km and the trunk section has a length of 80 km, thus giving the basin a circumference of just over 400 km. Again, the maximum depth is 150 m and the Ekman depth is 1 m. The numerical solutions were obtained on a two-dimensional grid with a mesh size of 4 km as used in Section 4.

The computed alongshore currents will be shown for points A and B of Fig. 7 which are located 10 km from the shore. These results are depicted on the left and right of Fig. 8, respectively. The solid curves refer to a symmetric, elongated basin with the shaded area of Fig. 7 going to zero, the dash–dot curves refer to Fig. 7a and the short dashes refer to Fig. 7b.

For the symmetric basin (solid curves), the results are similar to those for the circular basin (Figs. 5b and 6). The amplitude in point A is smaller than in point B due to the standing nature of the nearshore response. As in Fig. 6, this effect becomes stronger for shallower water or higher friction (not shown). The phase difference between the two points is ~27% of the forcing period for periods in the range of 5–15 days. Since the distance is only 20% of the circumference, the wave spends proportionally more time along the straight shores than along the end circles, similar to the different resonance periods on the lhs and rhs of Fig. 5. At 2 km offshore (not shown), the phase difference near resonance is only half as large as at 10 km and thus the response appears more like a standing wave as seen in Fig. 6 for the same offshore location.

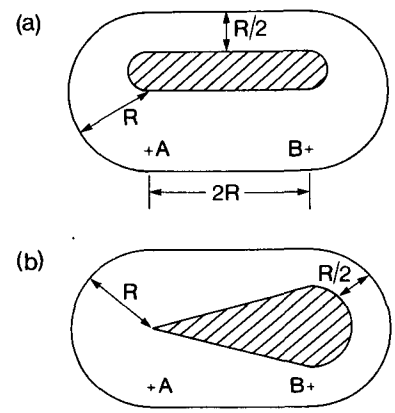

FIG. 7. Idealized elongated basins with latitudinal (a) and longitudinal (b) asymmetry. Depth is constant in shaded areas and parabolic in coastal zones.

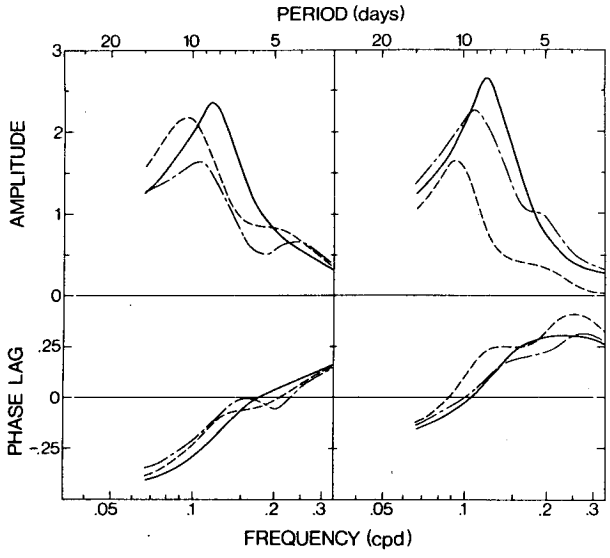

FIG. 8. Alongshore current in points A (left) and B (right) of basins of Fig. 7, subjected to wind from the left, uniform in space and periodic in time. Solid line is for symmetric elongated basin of Fig. 7 without shaded area, dash-dot line for basin of Fig. 7a and dashed line for basin of Fig. 7b. Radius 40 km, maximum depth 150 m, Ekman depth 1 m, offshore distance 10 km.

In case of latitudinal asymmetry (Fig. 7a, dash-dot curves of Fig. 8), the resonance period shifts by one day due to the effect of the narrower coastal zone at the opposite shore and the correspondingly longer normal mode period. The amplitude of the response is reduced as noted previously when comparing the solid curves of Figs. 3a and b. Furthermore, a secondary peak appears at approximately twice the resonance frequency, thus suggesting a wavelength equal to half the circumference. The phase difference between points A and B is reduced to 21% of the forcing period for periods longer than five days. This apparent agreement with the distance being 20% of the circumference, is in fact, the result of two opposing deviations. As in the symmetric case (solid lines), the wave moves slower along the straight parts of the shoreline, but due to the asymmetry, the wave moves faster over the wider coastal zone on the south side and spends only 40% of the time in the southern half of the basin.

The case of longitudinal asymmetry (Fig. 7b, dashed curves of Fig. 8), is essentially the same as the foregoing, but with the alongshore depth variation shifted by a quarter of the wavelength. As in Fig. 3b and 4, the amplitude response in the narrow coastal zone (point B) is reduced as compared to the wide coastal zone (point A). The resonance peaks shift to longer periods than in the symmetric basin (solid lines) similar to the shifts between the peaks of Fig. 3b and the solid line of Fig. 3a. Also, as in Fig. 3b, the resonance peaks appear to be determined by the average depth profile rather than the local bathymetry and hence tend to occur at more or less the same frequency at both points A and B. As noted for the shelf with alongshore depth variation, this result reflects a two-dimensional mode for this particular basin. The phase difference between points A and B is about 32% of the forcing period near the resonance frequency. This is greater than the corresponding value in the symmetric case which again agrees with Fig. 4 which shows that the phase lag increases between the wide and the narrow coastal zone and hence the wave slows down over this distance.

7. Comparison with observations

From 9 December 1973 to 18 March 1974, current measurements were made in the coastal zone off the city of Oshawa which is located on the northshore of Lake Ontario ~100 km from the western end of the lake. Currents were measured at 10 m below the surface and just above the bottom with horizontal separations of 1.5 km over a 10 km shore zone. The water depth varies more or less linearly from 15 m at the nearshore station to 65 m at the deepest station. Simultaneous wind observations are available from Toronto Island, approximately 50 km to the west. These winds were used to estimate stresses by the conventional formulation with a drag coefficient of 1.2×10^{-3} for wind speeds less than 10 m s^{-1}, linearly increasing to 2.4×10^{-3} at speeds of 20 m s^{-1}, and equal to the latter value for higher wind speeds. The stress vector, as well as the currents, were decomposed into components along and normal to the local shoreline. Energy spectra showed that low frequency currents in all stations were essentially parallel to the shoreline. Experiments with two-dimensional models of Lake Ontario showed that local currents induced by winds normal to the local shore were small compared to those induced by alongshore winds. This study will therefore concern itself with the response of alongshore currents to alongshore wind stress.

Although the bathymetry of Lake Ontario's north shore is quite uniform, the phase speeds of shelf waves are so sensitive to small depth variations that alongshore variations in wave speeds are substantial. This is illustrated in Fig. 9 which shows dispersion curves of topographic waves on the north shore of Lake Ontario between 78 and 79°W. The wavenumber is expressed in terms of the circumference of the lake, approximately 600 km, which obviously represents a long-wave cutoff for any shelf waves in Lake Ontario. Since the Oshawa experiment was located near 78.8°W, the corresponding first mode period would be greater than 10 days. However, as shown above, the resonance frequencies tend to represent the integrated effect of alongshore depth variations and hence resonance is expected to occur near 10 days. This period will be reduced even further if the effective wavelength is smaller than the circumference of

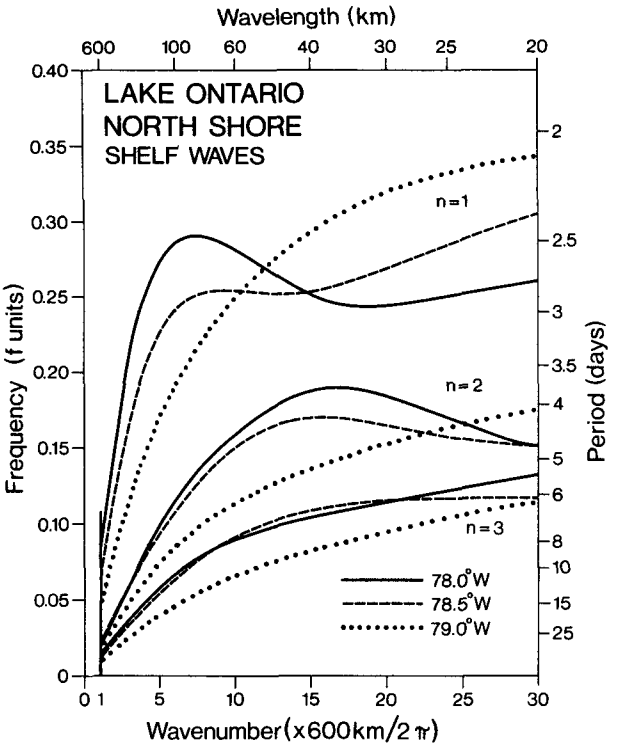

FIG. 9. Shelf wave dispersion curves for the north shore of Lake Ontario.

the lake. Indeed, Hamblin's (1972) numerical calculation of the rotational mode of Lake Ontario corresponding to the cubic mode of an elliptic paraboloid, produced a period of 10 days. Rao and Schwab (1976) found a mode with a similar period but suggested that another mode with twice this period was, by virtue of its spatial structure, more likely to be important for the low-frequency response of the lake. However, the period and the offshore structure of this mode are more similar to those of the second-mode shelf waves of Lake Ontario's north shore (Fig. 9). In any case, the results of numerical model verification studies (see, Simons, 1980) as well as the following model comparison, strongly suggest that the Hamblin mode is the one most readily excited by the wind and best suited to overcome effects of friction.

To compare the observations in Lake Ontario with the foregoing results for the resonant response of currents to wind, a two-dimensional, vertically-integrated model of Lake Ontario is employed. The numerical grid has a mesh size of 5 km and is aligned with the north shore. The wind is uniform in space and the bottom friction is formulated according to Ekman theory (3). Two versions of the model were compared. The first one is a free surface model with a single Richardson lattice, the second one is a rigid lid model. Differences between the results were found to be much smaller than effects of friction discussed here, so the following presentation will confine itself to the free surface model. The model results of interest are the alongshore currents in the grid points located 2, 7 and 12 km from the Oshawa shore with water depths of 16, 48 and 78 m respectively.

For a general time history of wind forcing, the response of the lake at a given location may be determined from a convolution integral involving the wind-stress and the unit impulse response. The latter is the response to a unit stress of 1 N m^{-2} applied over a unit time interval, say 1 hour. If one is concerned with model verification at a particular location, this method of calculation offers certain advantages since the complete two-dimensional model needs to be used only for computing the impulse response. The response of the alongshore current to a unit stress impulse of 1-hour duration is shown by the solid lines in Fig. 10 for the two model points nearest to the Oshawa shore. To illustrate effects of topographic waves, model results for the case of no rotation are shown by the dashed curves. Inspection of this figure shows that the most important effect of topographic waves is to cause a strong current reversal a few days after a wind impulse. It furthermore indicates that the wave is rapidly damped out and hence must be continually reinforced by wind impulses if it is to overcome effects of bottom friction.

The spectral response of the observed current to the observed wind forcing was estimated by taking the square root of the spectral energy ratio between

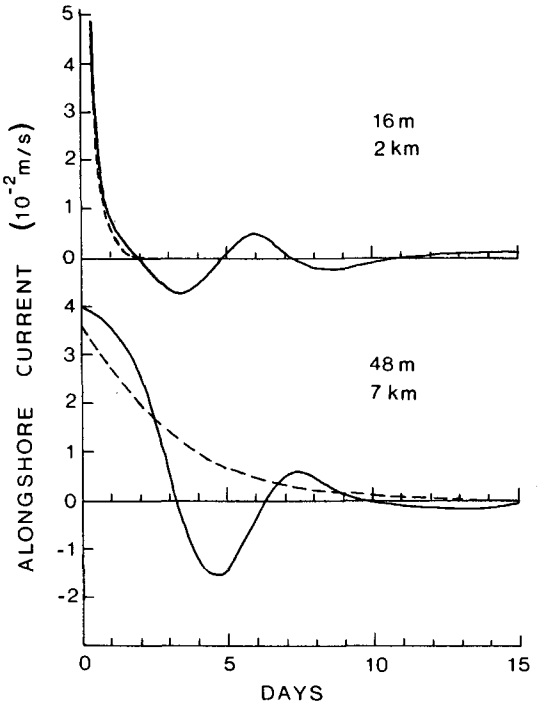

FIG. 10. Unit impulse response to 1 h wind for Lake Ontario coastal zone off Oshawa. Dashed line is solution without rotation.

currents and wind, together with the spectral coherence and phase between the wind and each individual current meter record. The results, as a function of frequency and distance from the Oshawa shore, are shown on the left-hand side of Fig. 11. These results refer to the bottom observations. Surface measurements show nearly identical phase lags and amplitude response shapes but the amplitudes are larger by as much as 20–40%. Coherence between wind and currents in this frequency range is ~0.9, a little higher for nearshore currents, a little lower for offshore currents.

The model response to wind, as a function of frequency, may be obtained by solving Eq. (5) for the basin of interest. However, since the impulse response was available for simulations in the time domain, this response was convoluted with periodic winds of the desired frequency and the resulting amplitude and phase response were determined by fitting a wave of the proper period to the computed current. The results for finite-depth Ekman friction (3) with Ekman depth of 2 m are shown in the middle panel of Fig. 11. The phase lags may be readily explained by realizing that the location of Oshawa is comparable to point B in the idealized basin of Fig. 7 with the corresponding results of Fig. 8b. The phase lags are thus larger than they would be at the mid-point of the north shore where the lag is expected to go to zero near the resonance period. The computed phase lags agree quite well with the observed ones. The amplitudes, however, increase towards the shore in contrast to the observed variation. This could be due to the lack of horizontal diffusion in the model or to an underestimation of frictional effects in shallow water.

For the present Ekman depth of 2 m, the finite depth formulation (3) is essentially similar to the deep-water approximation in the model grid points under consideration. In an effort to increase the nearshore friction, the shallow-water approximation was used with twice the Ekman depth. The results are presented on the right of Fig. 11. This friction appears to simulate the proper offshore variation of the currents although the overall damping appears overestimated. Another important discrepancy between the model and the observations is the exaggerated shift of the resonant response as a function of offshore distance. The shift is much greater than found in the foregoing idealized basins which is essentially due to the larger friction used here.

8. Momentum balance

A comparison of observed and computed currents in the time domain is shown in Fig. 12. The shallow-water approximation of Ekman friction with an Ekman depth of 4 m is used here. While the local current

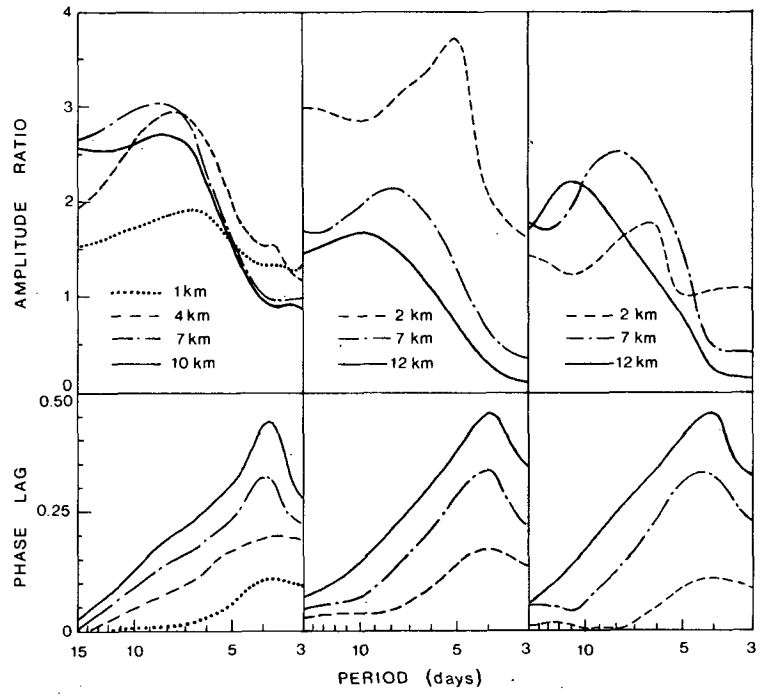

FIG. 11. Relation between alongshore current and alongshore windstress as a function of frequency. Left: observed in Lake Ontario coastal zone, 9 December 1973 to 3 March 1974. Middle: simulated by two-dimensional model with Ekman depth of 2 m. Right: simulated with Ekman friction for shallow water and Ekman depth of 4 m.

simulations are, at times, in error, it is interesting to note the satisfactory simulation of the offshore variation of alongshore currents. This would indicate that much of the local error is due to erroneous wind input.

If it is accepted that the two-dimensional model of Lake Ontario reproduces the major characteristics of the observed response of currents to wind, then the model offers an interesting opportunity to analyze the momentum balance associated with this response. In the literature some examples may be found of this type of momentum balance as calculated from observed quantities, but it is doubtful whether such terms as the pressure gradient and the Coriolis term can be properly evaluated. The alongshore pressure gradient is usually estimated by recourse to shore-based sea-level gauges, while the Coriolis term is obtained from the generally small deviation of the current from the alongshore direction. Thus, in a recent summary of such calculations, Allen and Smith (1981) showed that a large fraction of the variance of alongshore current accelerations and pressure gradients along the Oregon Coast can be explained by the wind but that the Coriolis term was not balanced by other estimated terms.

The alongsore momentum balance for the model results at the gridpoint closest to the shore is governed by wind and bottom stress. For the solution at 2 km shown in Fig. 12, the correlation between these two stresses is found to be equal to 0.88. The correlation of the alongshore pressure gradient with the wind is equal to 0.66, but the pressure gradient does not play an important role in this momentum balance since it is multiplied by the shallow nearshore depth. On the other hand, at the offshore station shown by the solid line of Fig. 12, the bottom stress is negligible

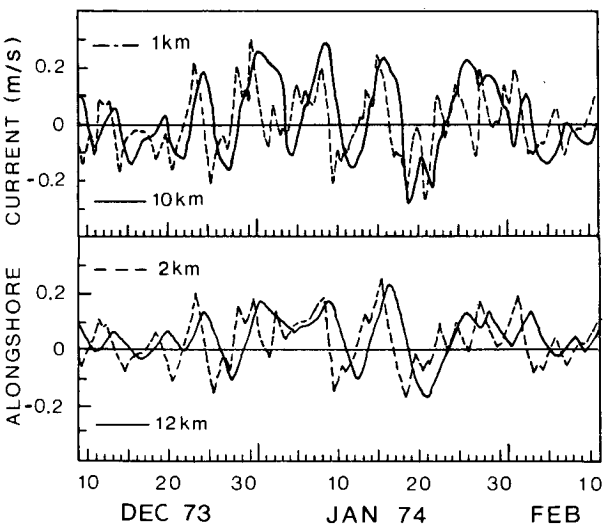

FIG. 12. Observed (above) and computed (below) currents in Lake Ontario coastal zone off Oshawa.

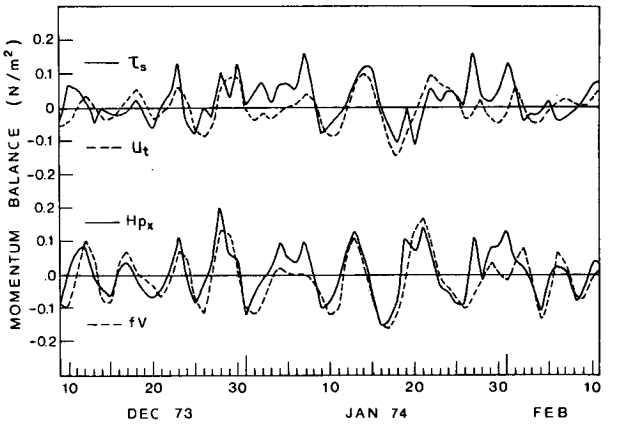

FIG. 13. Momentum balance for two-dimensional model at distance of 12 km from the north shore of Lake Ontario.

and all other terms are of equal magnitude as shown in Fig. 13. The pressure gradient is still correlated with the wind, the correlation coefficient being 0.57, but more important is its correlation with the Coriolis term which is as high as 0.74, while the correlation between the Coriolis term and the wind is only 0.14. In fact, as clearly seen in Fig. 13, the pressure gradient is largely canceled by the Coriolis term, thus pointing out the effects of topographic waves on the alongshore momentum balance some distance offshore. This is confirmed by comparing the alongshore pressure gradient at the nearshore station with that in the offshore station. The correlation coefficient is only 0.09, which indicates that shore-based sea level measurements may not be adequate to estimate the momentum balance in a station some 10 km offshore if topographic waves are present.

The cancelation of the pressure gradient by the Coriolis force may partly explain the apparent success of simple momentum balance models in simulating observed nearshore currents (e.g., Hickey, 1981). An example of a rather simple model of this kind is the one-dimensional channel model where the wind and bottom stress, integrated over the width of the channel, are balanced by an alongshore pressure gradient (Bennett, 1974). This model is known to produce good results for a closed basin when considering the short-term response to wind forcing, that is, before effects of topographic waves can become important. In this model, the cross-shore transport vanishes by virtue of the continuity equation and the boundary conditions, thus eliminating the Coriolis term from the alongshore momentum equation. Furthermore, since the averaged bottom stress tends to be small because of current reversals between opposing shores, the momentum equation takes on the approximate form

$$\frac{\partial U}{\partial t} \approx \left(1 - \frac{H}{\bar{H}}\right)\tau_{sx} - bHU, \qquad (8)$$

where the overbar denotes an average over the channel and b is the bottom stress coefficient defined by (3), which is approximated by the value $b = f\Delta H^{-2}$ in deep water and $b = 6f\Delta^2 H^{-3}$ in shallow water, where Δ is an Ekman depth defined as $\Delta = (\nu/2f)^{1/2}$.

While an equation such as (8) can never reproduce observed spectral current variations as shown in Fig. 11, it is of interest to test its performance in the time-domain. For this purpose, an equation of the form

$$\frac{\partial U}{\partial t} = \alpha\tau_{sx} - \beta U, \tag{9}$$

was integrated in time for a matrix of values of the coefficients α and β. For each of the observed current records, the pair of coefficients was found which minimized the rms difference between the solution and this observation. For the nearshore station with a depth of 16 m, the coefficients are $\alpha = 0.7$ and $\beta = 3 \times 10^{-5}$ s^{-1}, which is in reasonable agreement with (8) for an Ekman depth of 3–5 m. The solution in this case is nearly identical to the solution of the two-dimensional model shown in Fig. 12. However, for increasing distance offshore, the coefficient α approaches the value $\alpha = 1.0$ instead of decreasing according to (8) and the bottom friction decreases much slower with increasing H than suggested by the foregoing two-dimensional model verification. Although this result may at first seem surprising, it is consistent with the momentum balance of Fig. 13 as shown by the following experiment.

The solid line at the top of Fig. 14 shows computed currents at a distance of 12 km from the shore and at a depth of 78 m, as obtained from the two-dimensional model and as shown previously in Fig. 12. The dashed line at the top of Fig. 14 shows the solution of the channel model with the same bottom friction and with the pressure gradient opposing the wind stress in accordance with (8). This solution lacks the current reversals due to shelf waves and, as such, compares poorly with the observations shown in Fig. 12. The dashed line at the bottom of Fig. 12 shows the channel solution for the same bottom friction but without the effect of the pressure gradient which is equivalent to setting $\alpha = 1$ in (9). Finally, the solid line at the bottom of Fig. 12 is obtained from (8) or (9) without the pressure effect but with the bottom friction increased by a factor of four. It is seen that the last solution is remarkably similar to the first one. In summary, then, since the pressure gradient tends to be cancelled by the Coriolis term in the presence of shelf waves, a simple model without pressure gradients can give better results than the more complete model (8), if the bottom friction is manipulated to obtain the best fit to local observations.

The foregoing may also be illustrated by comparing the frequency response of the channel model with that of the two-dimensional model. The solid curve

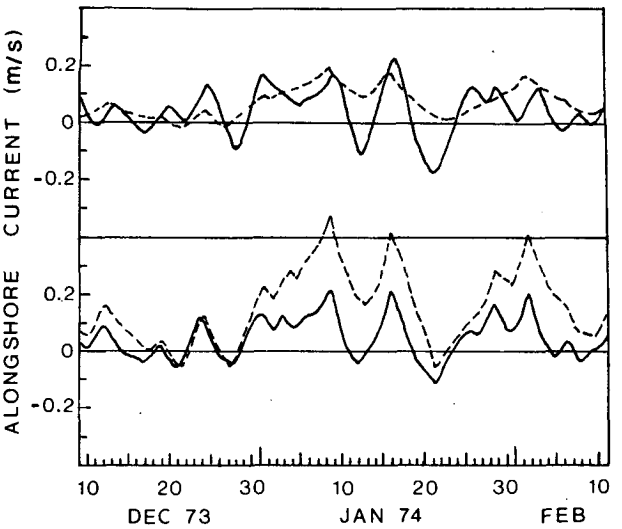

FIG. 14. Comparison of model currents, 12 km off Oshawa: (above, solid line) two-dimensional model of Fig. 12; (above, dashed) one-dimensional channel model equivalent to no-rotation; (below, dashed) model without rotation and without pressure gradient; (below, solid) same but four times greater Ekman depth.

of Fig. 15 is the response to wind at a distance of 12 km from the Oshawa shore as computed by the two-dimensional model and shown previously in Fig. 11. The short dashes in Fig. 15 represent the solution of the same model without rotation which may be verified to be quite similar to the analytical solution of the channel equation (8). The dash-dot curves in Fig. 15 are solutions of the same equation without pressure effects which effectively increases the forcing by a factor of $\bar{H}/(\bar{H} - H) = 4.5$. For periods near the resonance frequency, the response of the last model is remarkably similar to that of the two-dimensional model, both in amplitude and in phase. It must be concluded, however, that if the simple model in this case appears to produce acceptable solutions, this is the result of cancellation of opposing errors. Besides, for a closed basin, this model violates mass conservation principles.

9. Conclusions

The foregoing comparison of model results and observations indicates that topographic wave effects play an essential role in the barotropic response of nearshore currents to wind forcing. Analysis of alongshore momentum budgets shows that the alongshore pressure gradient, some distance offshore, tends to be cancelled by the Coriolis force and is poorly correlated with the nearshore pressure gradient. As a result, simple momentum balance models without topographic wave effects may appear to produce acceptable results if the pressure gradients are discarded and if the bottom stress is manipulated to obtain the best fit to local observations. It is concluded that such

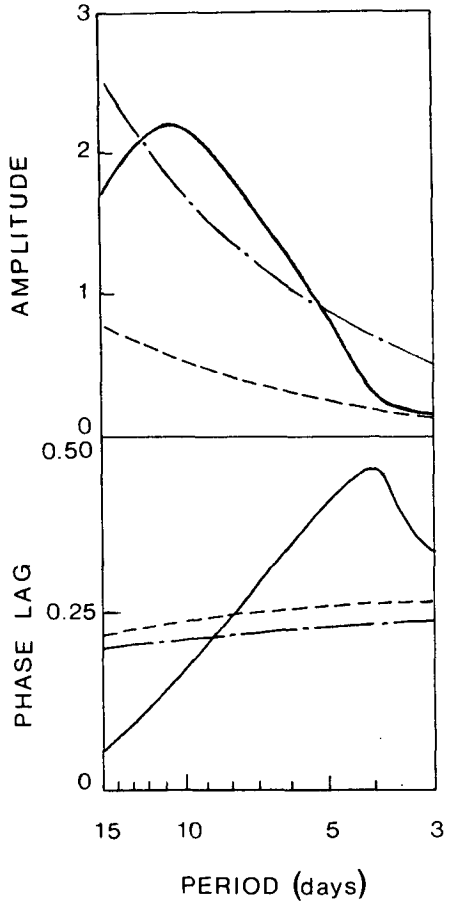

FIG. 15. Computed response of alongshore current to periodic wind at distance of 12 km from the north shore of Lake Ontario; (solid line) two-dimensional model, (dashed) no rotation, (dash-dot) no rotation and no pressure gradient.

model simulations are basically erroneous in concept. It is also suggested that shore-based water level gauges may give a poor estimate of the pressure gradient in the alongshore momentum balance some distance offshore.

Acknowledgments. The coastal climatology program of the Canadian National Water Research Institute was initiated by and carried out under the guidance of Dr. C. R. Murthy. The author thanks Dr. Murthy for making the data available and for offering valuable advice in the course of this study.

REFERENCES

Allen, J. S., 1980: Models of wind-driven currents on the continental shelf. *Annual Review of Fluid Mechanics,* Vol. 12, Annual Reviews, Inc., 389–433.

——, and R. L. Smith, 1981: On the dynamics of wind-driven shelf currents. *Phil. Trans. Roy. Soc. London,* **A302,** 617–634.

Ball, F. K., 1967: Edge waves in an ocean of finite depth. *Deep Sea Res.,* **14,** 79–88.

Bennett, J. R., 1974: On the dynamics of wind-driven lake currents. *J. Phys. Oceanogr.,* **4,** 400–414.

Birchfield, G. E., 1973: An Ekman model of coastal currents in a lake or shallow sea. *J. Phys. Oceanogr.,* **3,** 419–428.

——, and B. P. Hickie, 1977: The time-dependent response of a circular basin of variable depth to a wind stress. *J. Phys. Oceanogr.,* **7,** 691–701.

Brink, K. H., and J. S. Allen, 1978: On the effect of bottom friction on barotropic motion over the continental shelf. *J. Phys. Oceanogr.,* **8,** 919–922.

Clarke, A. J., 1977: Observational and numerical evidence for wind-forced coastal trapped long waves. *J. Phys. Oceanogr.,* **7,** 231–247.

Gill, A. E., and E. H. Schumann, 1974: The generation of long shelf waves by the wind. *J. Phys. Oceanogr.,* **4,** 83–90.

Hamblin, P. F., 1972: Some free oscillations of a rotating natural basin. Ph.D. thesis, University of Washington, 97 pp.

Hickey, B. M., 1981: Alongshore coherence on the Pacific Northwest continental shelf, January to April, 1975. *J. Phys. Oceanogr.,* **11,** 822–835.

Mysak, L. A., 1980: Recent advances in shelf wave dynamics. *Rev. Geophys. Space Phys.,* **18,** 211–241.

Rao, D. B., and D. J. Schwab, 1976: Two-dimensional normal modes in arbitrary enclosed basins on a rotating earth: Application to Lakes Ontario and Superior. *Phil. Trans. Roy. Soc. London,* **A281,** 63–96.

Saylor, J. H., J. C. K. Huang and R. O. Reid, 1980: Vortex modes in southern Lake Michigan. *J. Phys. Oceanogr.,* **10,** 1814–1823.

Simons, T. J., 1980: Circulation models of lakes and inland seas. *Can. Bull. Fish. Aquat. Sci.,* **203,** 146 pp.

Wang, D. P., 1980: Diffraction of continental shelf waves by irregular alongshore geometry. *J. Phys. Oceanogr.,* **10,** 1187–1199.